

CONTENTS

	Page
Acknowledgements	d
Abstract in Thai	f
Abstract in English	i
List of Tables	p
List of Figures	r
List of Abbreviations	x
List of Symbols	z
Statement of Originality in Thai	bb
Statement of Originality in English	cc
Chapter 1 Introduction and Research Objective	1
1.1 Introduction	1
1.2 Research objectives	2
1.3 Usefulness of the research	3
Chapter 2 Theoretical Background	4
2.1 Transparent conducting films	4
2.1.1 P-type semiconductor	5
2.1.2 N-type semiconductor	6

2.2	Oxide based materials	8
2.2.1	Indium tin oxide films	10
2.2.2	Zinc oxide films	13
2.3	Ultrasonic spray pyrolysis	16
2.4	Literature Review	20
2.4.1	Indium tin oxide	20
2.4.2	Zinc oxide	22
Chapter 3	Experimental Procedures	24
3.1	Film preparation	24
3.1.1	Substrate Cleaning	24
3.1.2	Film preparation	25
3.2	Film Characterization	26
3.2.1	X-ray diffraction (XRD) method	26
3.2.2	Scanning electron microscope (SEM)	28
3.2.3	Atomic force microscope (AFM)	31
3.2.4	UV visible spectrophotometer	33
3.2.5	Four point probe technique	35
Chapter 4	Results and Discussion (Part I): Indium Tin Oxide (ITO) Films	37
4.1	Film preparation	37
4.1.1	Starting solution preparation	37
4.1.2	Spray coating	38
4.2	Results and discussion	38
4.2.1	Thickness	39
4.2.2	Crystal structure	40
4.2.3	Morphology	42
4.2.4	Optical properties	46
4.2.5	Electrical properties	49

Chapter 5	Results and Discussion (Part II): ITO/Au/ITO Multilayer Films	51
5.1	Film preparation	51
5.1.1	Starting solution preparation	51
5.1.2	Film deposition	51
5.2	Results and discussion	53
5.2.1	Thickness	54
5.2.2	Crystal structure	55
5.2.3	Morphology	57
5.2.4	Optical properties	62
5.2.5	Electrical properties	65
5.2.6	Performance	66
Chapter 6	Results and Discussion (Part III): Mg Doped ZnO Films (I)	68
6.1	Film preparation	68
6.1.1	Starting solution preparation	68
6.1.2	Spray coating	69
6.2	Results and discussion	70
6.2.1	Thickness	70
6.2.2	Crystal structure	73
6.2.3	Morphology	76
6.2.4	Optical properties	87
6.2.5	Electrical properties	93
Chapter 7	Results and Discussion (Part IV): Mg Doped ZnO Films (II)	95
7.1	Film preparation	95
7.1.1	Starting solution preparation	95
7.1.2	Spray coating	96
7.2	Results and discussion	96
7.2.1	Thickness	97
7.2.2	Crystal structure	98

7.2.3	Morphology	100
7.2.4	Optical properties	103
7.2.5	Electrical properties	106
Chapter 8	Results and Discussion (Part V): In-Mg Codoped ZnO Films	107
8.1	Film preparation	107
7.1.1	Starting solution preparation	107
7.1.2	Spray coating	107
8.2	Results and discussion	108
8.2.1	Thickness	109
8.2.2	Crystal structure	110
8.2.3	Morphology	112
8.2.4	Optical properties	115
8.2.5	Electrical properties	117
Chapter 9	Conclusions	119
References		121
Curriculum Vitae		133

ลิขสิทธิ์มหาวิทยาลัยเชียงใหม่
 Copyright© by Chiang Mai University
 All rights reserved

LIST OF TABLES

		Page
Table 2.1	Type of oxide based materials, dopant elements and n-type TCO films	8
Table 2.2	The properties of TCO films achieved by different deposition techniques	17
Table 4.1	Specifications of materials and compositions of the starting solutions for ITO films used in this study	37
Table 4.2	Thickness of ITO films with different Sn concentrations	40
Table 4.3	Crystallite sizes of (222) and (400) planes of ITO films with different Sn concentrations	41
Table 5.1	Thicknesses of ITO/Au/ITO multilayer films with different Au intermediate layer thicknesses	55
Table 5.2	Crystallite size of (222) and (400) plane of ITO/Au/ITO multilayer films with different Au intermediate layer thicknesses	56
Table 5.3	The transmission coefficient at wavelength of 550 nm of ITO/Au/ITO multilayer films with difference Au intermediate layer thicknesses	66
Table 6.1	Specifications materials and compositions of the starting solutions for Mg doped ZnO films used in this study	69
Table 6.2	Thickness of Mg doped ZnO films with different Mg concentrations deposited on a glass substrates heated at 350-450°C	73

Table 6.3	Crystallite size of (002) and (101) plane of Mg doped ZnO films with different Mg concentrations deposited on a glass substrates heated at 350-450°C	76
Table 7.1	Specifications of materials and compositions of the starting solutions for Mg doped ZnO films used in this study	96
Table 7.2	Thickness of Mg doped ZnO films with different Mg concentrations	98
Table 7.3	Crystallite size of (002) and (101) plane of Mg doped ZnO films with different Mg concentration	99
Table 8.1	Specifications materials and compositions of the starting solutions of In-Mg codoped ZnO films used in this study	108
Table 8.2	Thickness of In-Mg codoped ZnO films different In concentrations	110
Table 8.3	Crystallite size of (002) and (101) planes of In-Mg codoped ZnO with different In concentration	111

LIST OF FIGURES

		Page
Figure 2.1	Phase space of binary oxides of TCO films	5
Figure 2.2	The schematic of a Si crystal lattice doped with B impurity atom	5
Figure 2.3	The schematic of band diagram of p-type semiconductor	6
Figure 2.4	The schematic of a Si crystal lattice doped with As impurity atom	7
Figure 2.5	The schematic of band diagram of p-type semiconductor	7
Figure 2.6	In ₂ O ₃ crystal structure: cubic (bixbyite-type) (a) and hexagonal (corundum-type) (b)	10
Figure 2.7	Cation sites: b site (a) and d site (b) in bixbyite type	11
Figure 2.8	Dependence of resistivity, carrier density, and Hall mobility on SnO ₂ content for the deposited ITO films. The substrate deposition temperature was kept at 250 °C and the oxygen pressure was 10 mTorr during deposition	12
Figure 2.9	Typical transmission, reflectance, and absorption spectra for the ITO film grown at 200 °C and 10 mTorr of oxygen. The film thickness was 300 nm	13
Figure 2.10	ZnO crystal structure: cubic rocksalt (a), cubic zinc blend (b) and hexagonal wurtzite (c) when shaded gray and black sphere denoted Zn and O atom, respectively	14
Figure 2.11	The hexagonal wurtzite structure model of ZnO. The tetrahedral coordination of Zn-O is shown	14
Figure 2.12	Carrier density, mobility (a) and resistivity (b) of undoped ZnO film with different oxygen pressure	15
Figure 2.13	Typical transmittance, reflectance, and absorbance spectra for the Al doped ZnO film	16
Figure 2.14	The mechanisms of particle formation and decomposition reaction	19

Figure 2.15	Schematic representations of spray pyrolysis deposition apparatus	19
Figure 2.16	The dispersion of particle in droplet of ultrasonic nozzle and air spray nozzle	20
Figure 3.1	Schematic diagram of the substrate cleaning	24
Figure 3.2	Schematic diagram of film coating	25
Figure 3.3	Scheme of the X-ray diffraction geometry	27
Figure 3.4	XRD pattern of ZnO powder	27
Figure 3.5	X-ray diffractometer (PANalytical, X'pert Pro MPD)	28
Figure 3.6	Schematic diagram of SEM	29
Figure 3.7	Electrons produced in SEM	29
Figure 3.8	Scanning electron microscope	30
Figure 3.9	The Image of AFM probe	31
Figure 3.10	Principle of AFM	32
Figure 3.11	Digital Instruments Nanoscope III Scanning Probe Microscope	32
Figure 3.12	Electromagnetic spectrum	33
Figure 3.13	Schematic diagram of the absorption process	33
Figure 3.14	PerkinElmer Lambda 35 UV/VIS Spectrophotometer	35
Figure 3.15	Four point probe technique	35
Figure 3.16	Hewlett Packard 3458A multimeter	36
Figure 4.1	Schematic diagram of ITO film preparation	38
Figure 4.2	Images of ITO films with different Sn concentrations deposited on glass substrates	39
Figure 4.3	SEM cross section microstructures of ITO films with different Sn concentrations deposited on glass substrates	39
Figure 4.4	The XRD patterns of ITO films with different Sn concentrations	41
Figure 4.5	SEM images of ITO films with different Sn concentrations	43
Figure 4.6	AFM images of top ITO films with different Sn concentrations	44
Figure 4.7	Average grain size and surface roughness of ITO films with different Sn concentrations	46
Figure 4.8	Transmittance (a) and absorbance (b) spectra of ITO films with different Sn concentrations	47

Figure 4.9	The $(\alpha h\nu)^2$ versus $h\nu$ plots (a) and the band gap of ITO films with different Sn concentrations	48
Figure 4.10	The sheet resistance and the resistivity of ITO films with different Sn concentrations	50
Figure 5.1	Schematic diagram of ITO/Au/ITO multilayer film preparation	52
Figure 5.2	Image of ITO/Au/ITO multilayers films with different Au intermediate layer thicknesses	53
Figure 5.3	The cross section microstructures of ITO/Au/ITO multilayers films with different Au intermediate layer thicknesses	54
Figure 5.4	XRD patterns of ITO/Au/ITO multilayer film with different Au intermediate layer thicknesses	56
Figure 5.5	SEM images of ITO/Au/ITO multilayer films with different Au intermediate layer thicknesses	57
Figure 5.6	AFM images of ITO/Au/ITO multilayer films with different Au intermediate layer thicknesses	58
Figure 5.7	Average grain size and surface roughness of ITO/Au/ITO multilayer films with different Au intermediate layer thicknesses	59
Figure 5.8	AFM images of Au layer with different Au layer thicknesses	60
Figure 5.9	Average grain sizes and surface roughness of Au layer with different Au layer thicknesses	62
Figure 5.10	Transmittance (a) and absorbance (b) spectra of ITO/Au/ITO multilayer films with different Au intermediate layer thicknesses	63
Figure 5.11	The $(\alpha h\nu)^2$ versus $h\nu$ plots (a) and the band gap of ITO/Au/ITO multilayer films with different Au intermediate layer thicknesses	64
Figure 5.12	The sheet resistance and the resistivity of ITO/Au/ITO multilayer films with difference Au intermediate layer thickness	65
Figure 5.13	The figure of merit of ITO/Au/ITO multilayer films with different Au intermediate layer thicknesses	67
Figure 6.1	Schematic diagram of Mg doped ZnO film preparation	69

Figure 6.2	The appearance of Mg doped ZnO films with different Mg concentrations deposited on glass substrates heated at 350-450°C	70
Figure 6.3	SEM cross section microstructures of Mg doped ZnO films with different Mg concentrations deposited on glass substrates heated at 350°C (a), 400°C (b) and 450°C (c)	71
Figure 6.4	The XRD patterns of Mg doped ZnO films with different Mg concentrations on glass substrate deposited on a glass substrates heated at 350°C (a), 400°C (b) and 450°C (c)	75
Figure 6.5	Fracture surface of microscope glass substrate	75
Figure 6.6	SEM images of Mg doped ZnO films with different Mg concentrations deposited on a glass substrates heated at 350°C (a), 400°C (b) and 450°C (c)	77
Figure 6.7	AFM images of Mg doped ZnO films with different Mg concentrations deposited on a glass substrates heated at 350°C (a), 400°C (b) and 450°C (c)	80
Figure 6.8	Average grain size and surface roughness of Mg doped ZnO films with different Mg concentrations deposited on a glass substrates heated at 350 - 450°C	86
Figure 6.9	Transmittance spectra of Mg doped ZnO with different Mg concentrations deposited on a glass substrates heated at 350°C (a), 400°C (b) and 450°C (c)	87
Figure 6.10	Absorbance spectra of Mg doped ZnO films with different Mg concentrations deposited on a glass substrates heated at 350°C (a), 400°C (b) and 450°C (c)	89
Figure 6.11	The $(\alpha h\nu)^2$ versus $h\nu$ plots of Mg doped ZnO films with different Mg concentrations deposited on a glass substrates heated at 350°C (a), 400°C (b) and 450°C (c) and band gap (d) of these films	91
Figure 6.12	Sheet resistance (a) and resistivity (b) of Mg doped ZnO films with different Mg concentrations deposited on a glass substrates heated at 350-450°C	93

Figure 7.1	The appearance of Mg doped ZnO films with different Mg concentrations	96
Figure 7.2	The cross section microstructures of Mg doped ZnO films with different Mg concentrations	97
Figure 7.3	The XRD patterns of Mg doped ZnO films with different Mg concentrations	99
Figure 7.4	SEM images of Mg doped ZnO films with different Mg concentrations	100
Figure 7.5	AFM images of Mg doped ZnO films with different Mg concentrations	101
Figure 7.6	Average grain size and surface roughness of Mg doped ZnO films with different Mg concentrations	103
Figure 7.7	Transmittance (a) and absorbance (b) spectra of Mg doped ZnO films with different Mg concentrations	104
Figure 7.8	The $(ah\nu)^2$ versus $h\nu$ plots of Mg doped ZnO films with different Mg concentrations (a) and band gap (d) of these films	105
Figure 7.9	The sheet resistance and the resistivity of of Mg doped ZnO films with different Mg concentrations	106
Figure 8.1	The appearance of In-Mg codoped ZnO films with different In concentrations	108
Figure 8.2	The cross section microstructures of In-Mg codoped ZnO films with different In concentrations	109
Figure 8.3	The XRD patterns of In-Mg codoped ZnO films with different In concentrations	111
Figure 8.4	SEM images of Mg doped ZnO films with different In concentrations	112
Figure 8.5	AFM images of In-Mg codoped ZnO with different In concentrations	113
Figure 8.6	Average grain size and surface roughness of In-Mg doped ZnO films with different In concentrations	115
Figure 8.7	Transmittance (a) and absorbance (b) spectra of In-Mg cpodoped ZnO films with different In concentrations	116

- Figure 8.8 The $(\alpha h\nu)^2$ versus $h\nu$ plots of In-Mg codoped ZnO with different Mg concentrations (a) and band gap (b) of these films 117
- Figure 8.9 The sheet resistance and the resistivity of of In-Mg codoped ZnO with different In concentration 118

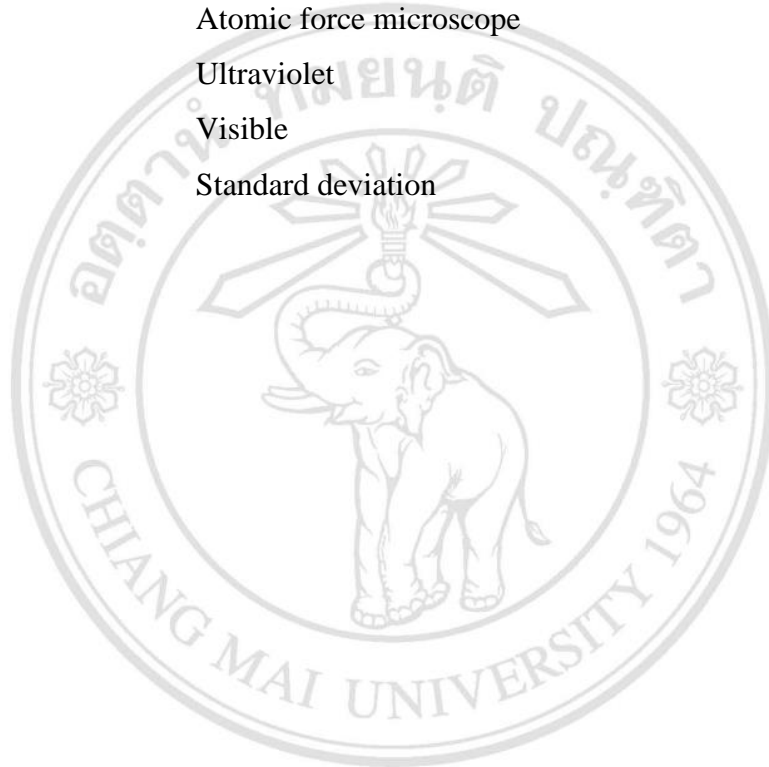


ลิขสิทธิ์มหาวิทยาลัยเชียงใหม่
Copyright© by Chiang Mai University
All rights reserved

LIST OF ABBREVIATIONS

a-Si:H	Hydrogenated amorphous silicon
$\mu\text{c-Si:H}$	Microcrystalline silicon
TCO	Transparent conductive oxide
In_2O_3	Indium oxide
SnO_2	Tin oxide
CdO	Cadmium oxide
ZnO	Zinc oxide
ITO	Tin doped indium oxide or indium tin oxide
ITiO	Titanium doped indium oxide
ATO	Antimony doped tin oxide
FTO	Fluorine doped tin oxide
CdO: Sn	Tin doped cadmium oxide
Cd ₀ : Al	Aluminium doped cadmium oxide
AZO	Aluminium doped zinc oxide
GZO	Gallium doped zinc oxide
CuAlO_2	Copper aluminium oxide
CuScO_2	Copper scandium oxide
CuYO_2	Copper yttrium oxide
CuInO_2	Copper indium oxide
CuGaO_2	Copper gallium oxide
CuCrO_2	Copper chromium oxide
$\text{Ca}_2\text{Al}_{1.5}\text{Fe}_{0.5}\text{SiO}_7$	Calcium aluminium iron silicate
CVD	Chemical vapor deposition
MBE	Molecular beam epitaxy
PLD	Pulsed laser deposition
RF	Radio frequency
DC	Direct current

HCl	Hydrochloric
DI	Deionized
XRD	X-ray diffraction
JCPDS	Joint Committee on Powder Diffraction Standards
FWHM	Full width at half maximum
SEM	Scanning electron microscope
BSEs	Backscattered electron
AFM	Atomic force microscope
UV	Ultraviolet
VIS	Visible
SD	Standard deviation



ลิขสิทธิ์มหาวิทยาลัยเชียงใหม่
 Copyright© by Chiang Mai University
 All rights reserved

LIST OF SYMBOLS

Ω	Ohm
V	Volt
s	Second
min	Minute
h	Hour
Hz	Hertz
S	Siemens
K	Kelvin
$^{\circ}\text{C}$	Degree Celsius
g	gram
cm	Centimeter
nm	Nanometer
μm	Micrometer
\AA	Angstrom
E_g	Energy band gap or band gap (eV)
σ	Conductivity (S)
ρ	Resistivity ($\Omega\cdot\text{cm}$)
R_s	Sheet resistance (Ω/sq)
N	Carrier concentration (cm^{-3})
μ	Hall mobility (cm^2/Vs)
A	Absorbance
T	Transmittance
R	Reflectance
α	Absorption coefficient
I	Transmitted radiation
I_0	Incident radiation
d	Spacing of planes of atom

θ	Angle of diffraction
λ	Wavelength
G	Crystalline size
β	FWHM which has maximum intensity
E	Energy (eV)
h	Plank's constant
ν	Photon frequency
c	Speed of light
t	Thickness
Φ_{TC}	Figure of merit
at. %	Atomic percentage



ลิขสิทธิ์มหาวิทยาลัยเชียงใหม่
 Copyright© by Chiang Mai University
 All rights reserved

ข้อความแห่งการริเริ่ม

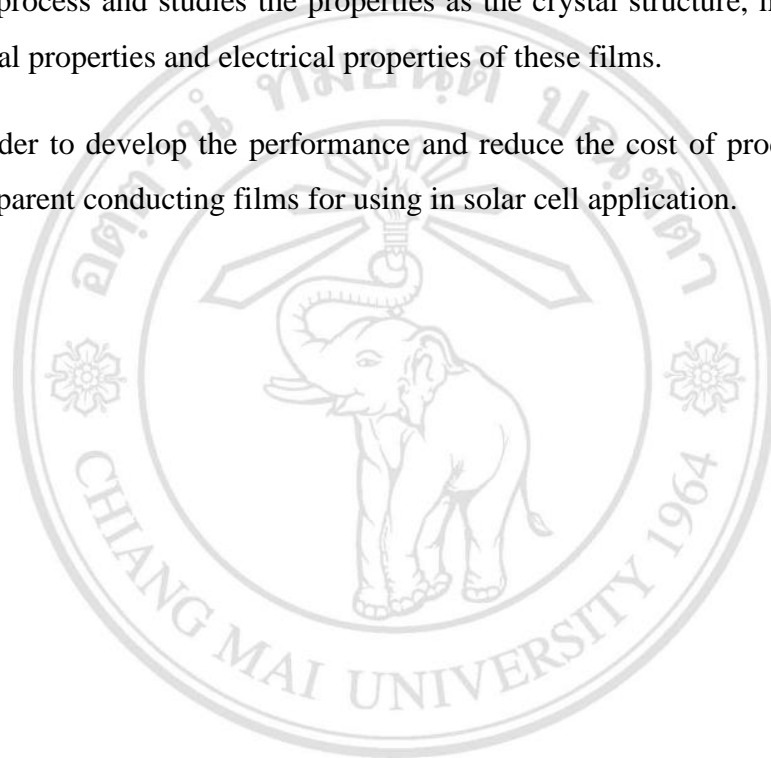
- 1) วิทยานิพนธ์นี้ได้นำเสนอการผลิตฟิล์มนำไฟฟ้าแบบโปร่งใส ด้วยวิธีการที่ใช้ต้นทุนต่ำและศึกษาสมบัติต่างๆ ได้แก่ ความเป็นผลึก โครงสร้างทางจุลภาค สมบัติทางแสง และสมบัติทางไฟฟ้าของฟิล์มนำไฟฟ้าแบบโปร่งใส
- 2) เพื่อพัฒนาประสิทธิภาพและลดต้นทุนการผลิตฟิล์มนำไฟฟ้าแบบโปร่งใส สำหรับประยุกต์ใช้งานด้านเซลล์แสงอาทิตย์



ลิขสิทธิ์มหาวิทยาลัยเชียงใหม่
Copyright© by Chiang Mai University
All rights reserved

STATEMENTS OF ORIGINALITY

1. This thesis presents the fabrication of transparent conducting films with low cost process and studies the properties as the crystal structure, microstructure, optical properties and electrical properties of these films.
2. In order to develop the performance and reduce the cost of production of the transparent conducting films for using in solar cell application.



ลิขสิทธิ์มหาวิทยาลัยเชียงใหม่
Copyright© by Chiang Mai University
All rights reserved